YRiS Yellow River Studies

News Letter Vol.2

March 1, 2004

Surface radiation budget over China

Kazuaki Kawamoto[1], Jianqing Xu[2] and Tadahiro Hayasaka[1]

1 Research Institute for Humanity and Nature
2 Frontier Research System for Global Change

The radiation budget at the surface is crucial for determining the evapotranspiration and calculation with numerical hydrological models. Here we introduce two surface radiative budget estimates that were obtained independently. One is with satellite data, and the other is using routine meteorological observations. Comparisons between these two datasets were made at several stations, and room for improvement of both methods was suggested.

1. Surface radiative flux estimated by satellite measurements

We adopt a method developed by NASA Langley Research Center as using satellite data. This is called LPSA (Langley Parameterization for Shortwave Approximation) (Gupta et al. 1999). LPSA uses cloud information such as the cloud optical depth, cloud top height, cloud amount and so on) from ISCCP (International Satellite Cloud Climatology) and meteorological parameters like water vapor amount and temperature profiles, and then determines the surface radiative flux empirically. Figure 1 illustrates examples of the monthly-mean surface shortwave radiative flux (hereafter referred to as S(Langley) for January, April, July and October in 1994. We find substantial difference between four panels due to accompanying seasonal changes of the solar incidence, wind pattern and cloud system. This dataset is prepared from July 1983 to October 1995.

2. Surface radiative flux estimated by routine meteorological observation

The surface radiation calculated by routine meteorological observations (hereafter referred to as S(N)) is formulated using the sunshine duration measured by sunshine recorders for all sky cases (clear and cloudy). Coefficients of Jordan sunshine recorders take the surface air pressure into account (Kondo 1994). S(N) is parameterized by the precipitable water and surface air pressure for clear sky cases. As the atmospheric turbidity, results of Robinson (1966) were assumed. Figure 2 shows the time-series of S(N) in Beijing from 1983 to 1995 which is the same period as that of S(Langley). Although values seem to have a decreasing trend generally, we need to perform detailed analyses on the long-term changes of the humidity and cloud properties. This dataset is prepared for more than 30 years, from 1970 to the present in China (Xu et al. 2004).

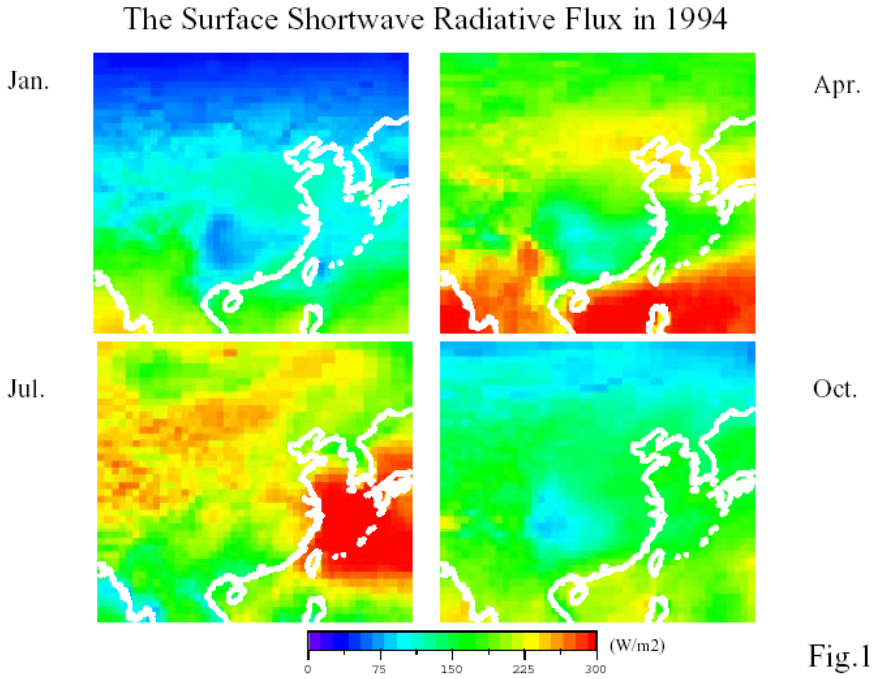

Fig.1

Fig.1 Monthly-mean downward shortwave radiative fluxes at the surface over China for January, April, July and October in 1994.

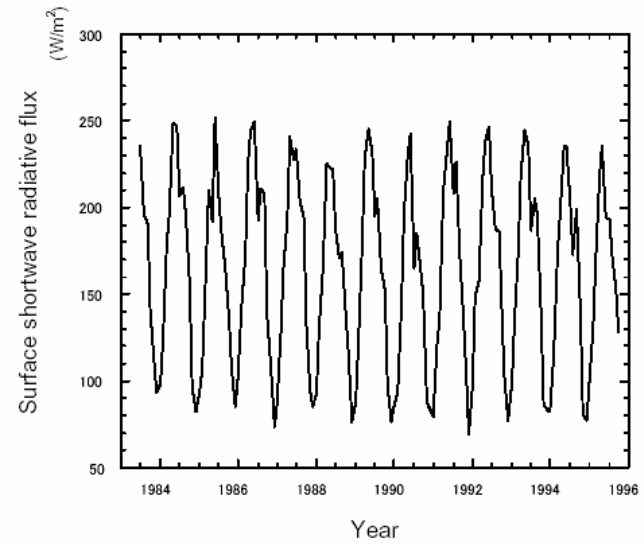

Fig. 2

Fig.2 Time-series of S(N) in Beijing from 1983 to 1995.

3. Comparisons of the two datasets at several stations and the geographical features

We made a comparison between the two datasets. Figures 3 presents time series of Beijing, Hailar and Lhasa cases, respectively. S(Langley) is systematically larger for Beijing case, and both methods are almost the same for Hailar case, and S(N) is larger on the whole for Lhasa case. Figure 4 shows a map of the observation points with results of the comparison. From this figure, we find following geographical features, that is,

S(Langley) is larger in big cities like Beijing and Shanghai, and both methods are almost the same in moderately-sized cities such as Hailar, and S(N) is larger in the west area near the Tibetan plateau. These features suggest room for improvement of both methods such as validity of the assumption about aerosol properties of big cities in estimating S(N) and topographical treatment of the west area in estimating S(Langley).

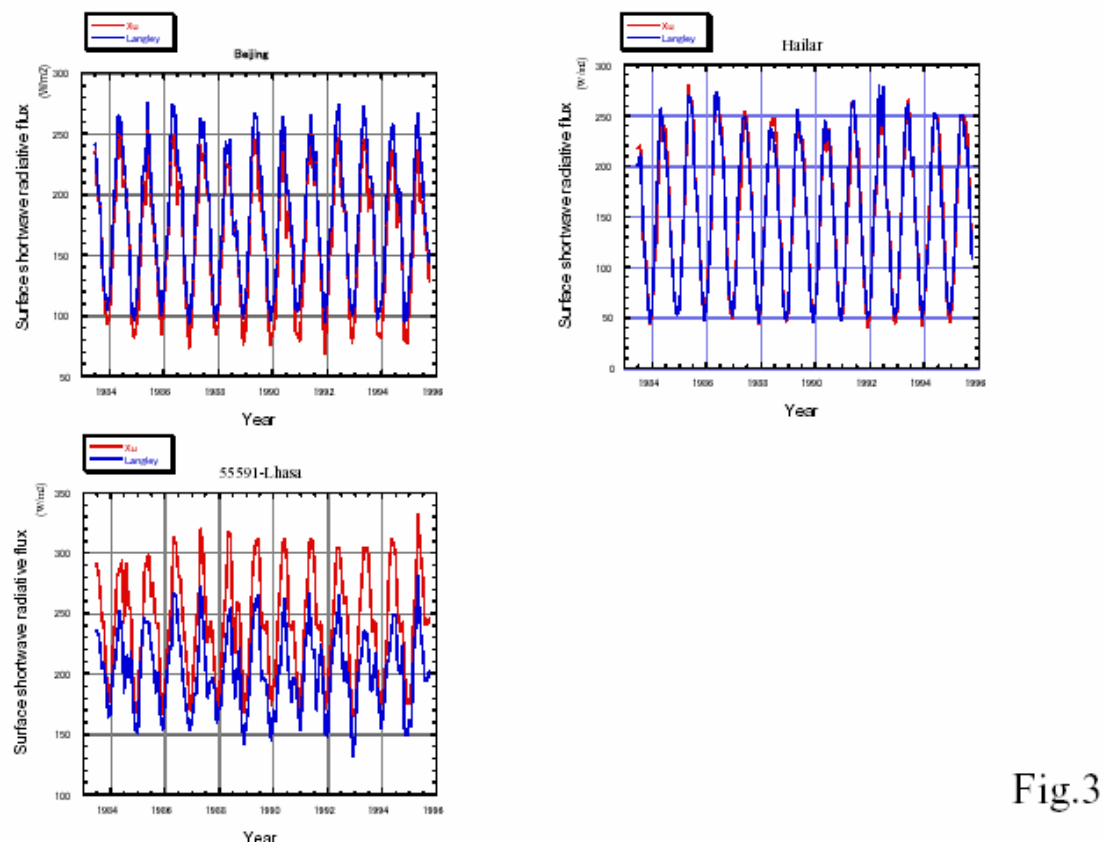

Fig.3

Fig.3 Time-series of the comparisons between S(N) and S(Langley) from 1983 to 1995 for Beijing, Hailar and Lhasa.

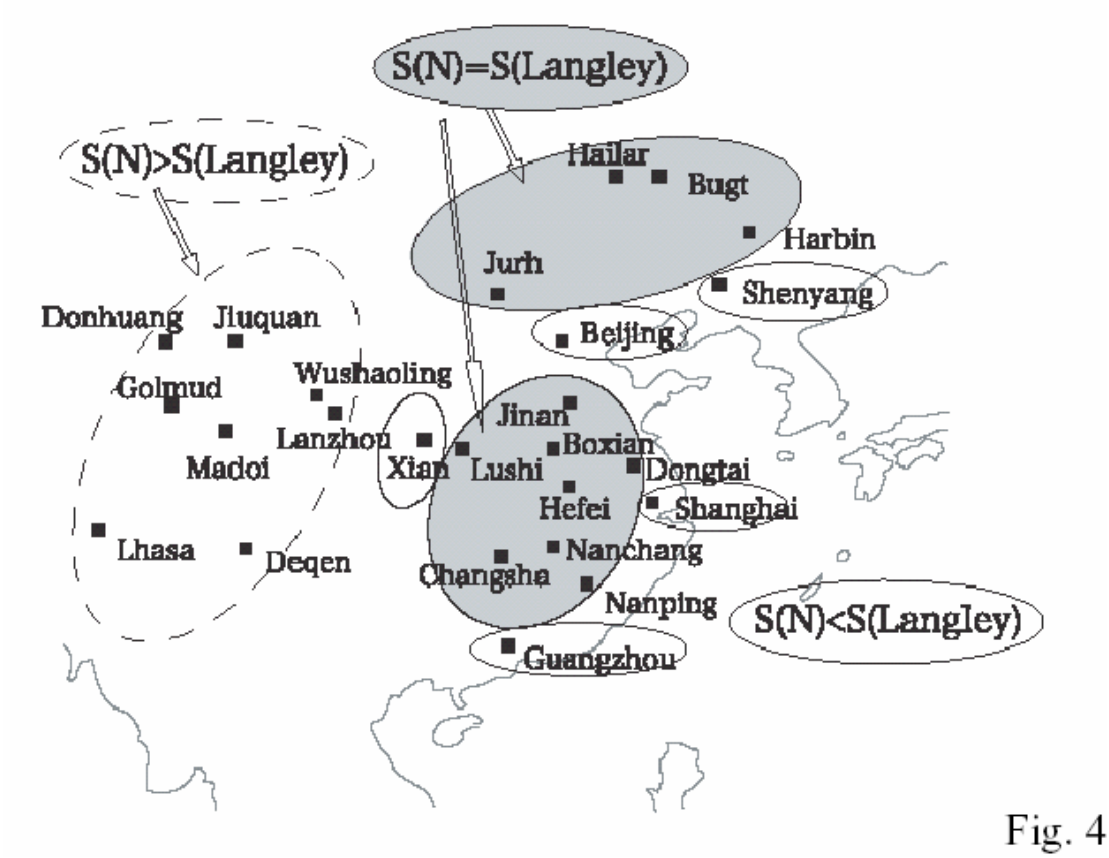

Fig.4 Geographical features of the comparison between S(N) and S(Langley)

References

Gupta, S. K., N. A. Ritchey, A. C. Wilber, C. H. Whitlock, G. G. Gibson, and P. W. Stackhouse Jr., 1999: A climatology of surface radiation budget derived from satellite data. *J. Climate*, **12**, 2691-2710.

Kondo, J., 1994: Meteorology of the Water Environment | Water and Heat Balance of the Earth's Surface. Asakura Shoten Press, Japan, 348pp., (in Japanese).

Robinson, N., Ed., 1966: Solar Radiation. Elsevier, 347pp.

Xu, J., T. Hayasaka, K. Kawamoto, S. Haginoya, 2003, An estimation of downward surface radiation over China, in preparation.

Progress Report on the Construction of the Daily Precipitation Analyses Over China

Pingping Xie*, Mingyue Chen*, and Akiyo Yatagai#

* NOAA/NWS Climate Prediction Center
# Research Institute for Humanity and Nature

1. Introduction

As part of the Yellow River Project, a suite of daily precipitation analyses products are being constructed for potential applications in meteorological, hydrological and water resources research. The products suite, designed to best take advantage of the available information to meet the needs for various programs, is comprised of three major components; i.e. 1) a gauge-based analysis on a 0.5^o lat/lon grid over the East Asia (70^oE – 140^oE; 0^o-60^oN) for an extended period from 1961 to the present (the Base Product); 2) a gauge-based analysis on 0.1^o lat/lon grid over the Yellow River basin for the same period (the Derived Product); and 3) a satellite-gauge merged analysis on a 0.25^o lat/lon grid over the East Asia for a recent period (the Merged Product).

The gauge-based analyses are the mainstay of the products suite, both for its extended temporal coverage and for its role in determining the magnitude in the merged analysis. In this article, we will report the recent progress on the construction of the gauge-based analyses of daily precipitation over the East Asia.

2. Methodology

The overall strategy for constructing the daily precipitation analyses is a modification of Chen et al. (2002), which was originally designed for gauge-based analyses of monthly precipitation over the global land areas.

The construction of the daily precipitation is composed of three steps. First, a gridded analysis of daily precipitation climatology is created for each of the 365 calendar days by interpolating the long-term mean daily precipitation observations at available gauge stations. An analyzed field of the ratio between the daily observation and daily climatology is then generated from the corresponding values at all available stations. The analysis of total daily precipitation is finally defined by multiplying the analyzed daily climatology with the ratio.

In creating the products suite, the analysis is first produced on a 0.05^o lat/lon grid over the entire East Asia domain. The Base Product and the Derived Product are then computed by averaging the values at the 0.05^o lat/lon resolution. A gauge-based analysis on 0.25^olat/lon is also created for use as input to the Merged Product, ensuring the consistency between the gauge-based analyses and the merged analysis.

3. Gauge Data

Station observations of daily precipitation from three individual data sets are used to construct the gauge-based analyses over the East Asia. These are the Global Telecommunication System (GTS) daily summary files archived by the NOAA Climate Prediction for a period from 1977 to the present; a personal collection of Chinese daily observations (CHN) for a period from 1951 to the present; and the daily gauge data from the Chinese Yellow River Commission (YRC) for a period from 1930S to 1997. Since most of the GTS stations are included in the CHN data set, only daily observations from CHN and YRC data sets are used inside China, while the GTS gauge data are used over the regions outside China. When combined, observations of daily precipitation at over 2500 stations are available over the East Asia domain. Fig.1 shows gauge locations from the individual and the combined data sets. Reasonable gauge coverage is available over most of the land areas of the East Asia domain, while network density is very high along the Yellow River, making it possible to creating a high resolution precipitation analysis with reliable quality over the region.

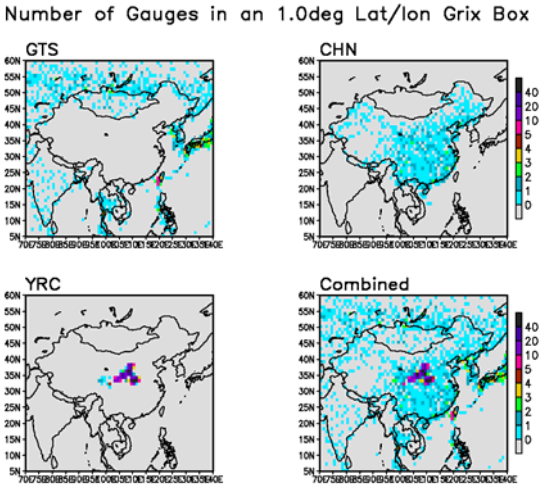

Figure 1. Number of gauges in each 1.0° lat/lon grid box as from the individual and the combined data sets.

4. Preliminary Result

A test version of the gauge-based analyses of daily precipitation has been generated for a 5-year period from 1994 to 1998 for quantitative examinations. Presented in fig.2 is an animation of the daily precipitation maps for a 31-day period from July 1 –31, 1997. Day-to-day variations of precipitation are well captured by this test product.

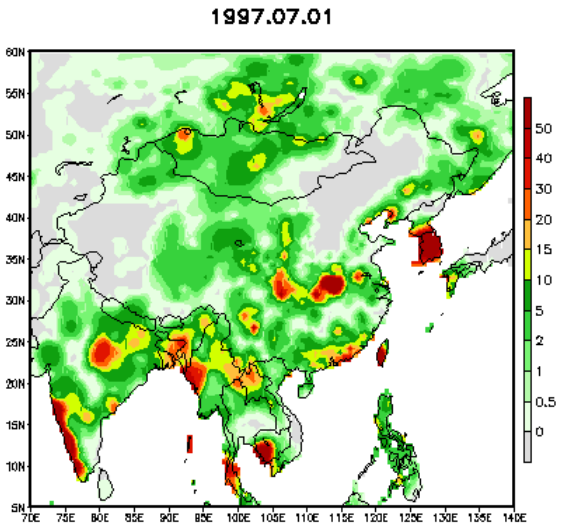

Figure 2: An animation of daily precipitation maps (mm/day) for a 31-day period from July 1 – 31, 1997.

5. Future Plan

Work is underway toward the completion of the gauge-based analyses for the Yellow River Project. In addition to the quantitative examinations for the test products for the 5-year period as mentioned above, our future work will focus on:

1) collecting station data from more stations;
2) improving the daily precipitation climatology with orographic consideration; and;
3) modifying the interpolation algorithm for better quantitative accuracy.

Your comments, suggestions, and cooperation are highly appreciated.

6. References

Chen, M., P. Xie, and J.E. Janowiak, and P.A. Arkin, 2002: Global Land Precipitation: A 50-yr Monthly Analysis Based on Gauge Observations, *J. Hydrometeor.*, **3**, 249 – 266.

Interannual variability in the hydrological budget over the Yellow River

Akiyo Yatagai (Research Institute for Humanity and Nature)

1. Introduction

Since the late 1990s, reanalysis of meteorological data using observations and a data assimilation scheme in a fixed global weather forecasting model has created dynamically consistent sets of historical atmospheric data (Kalnay et al., 1996; Gibson et al., 1997). The European Centre for Medium-Range Weather Forecasts (ECMWF) and National Centers for Environmental Prediction (NCEP) have both produced second generation reanalyses. Reanalysis data were used in this study to investigate interannual variability in the hydrological budget over the Yellow River. Analyses derived from the first ECMWF reanalysis (ERA15) are reported here. Analyses using the ECMWF 40-year reanalysis (ERA40, Simmons and Gibson 2000) are now underway.

2. Atmospheric moisture flux and hydrological budget

Figure 1 shows 15-year averages of atmospheric moisture content (precipitable water) and vertically integrated moisture flux over mid-latitudes of Eurasia. These values were computed using the first ECMWF reanalysis (ERA15). Computation details are in Yatagai (2003). The moisture flux vector (Q_λ, Q_φ) facilitates a computation of atmospheric moisture convergence
$-\nabla_H \cdot \mathbf{Q}$. If the time rate of change of liquid and solid water and their horizontal transports are neglected (Peixoto and Oort 1992), then $-\nabla_H \cdot \mathbf{Q} \fallingdotseq$ (Precipitation) – (Evapotranspiration) for spatial and temporal averages over a large area at

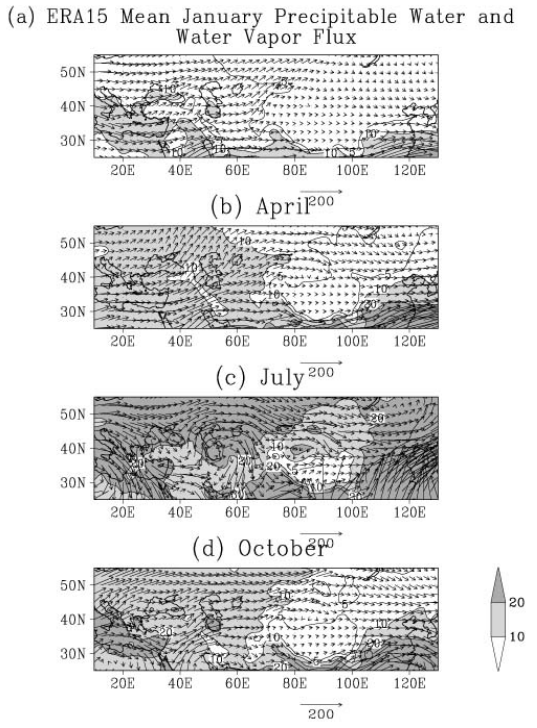

Fig. 1 Climatological mean precipitable water and vertically integrated moisture flux for (a) January, (b) April, (c) July and (d) October.

monthly to seasonal time scales.

This equation yields an estimate of evapotranspiration if regional mean precipitation data are known. Figure 2 shows the annual cycle of $-\nabla_H \cdot \mathbf{Q}$ (moisture convergence) and precipitation (from CPC Merged Analysis of Precipitation (CMAP), Xie and Arkin, 1997) for the large subregions shown in Figure 3 (dotted box). Details are given in Yatagai (2003).

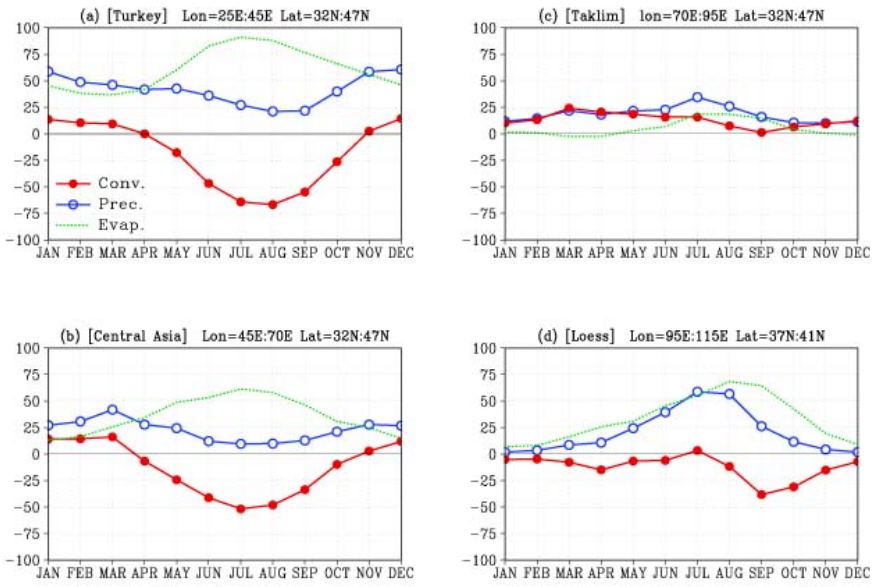

Fig.2 Annual cycle of $-\nabla_H \cdot Q$ and CMAP precipitation for subregions (a) Turkey, (b) central Asia, (c) the Taklimakan Desert, and (d) the Loess Plateau (mm/month).

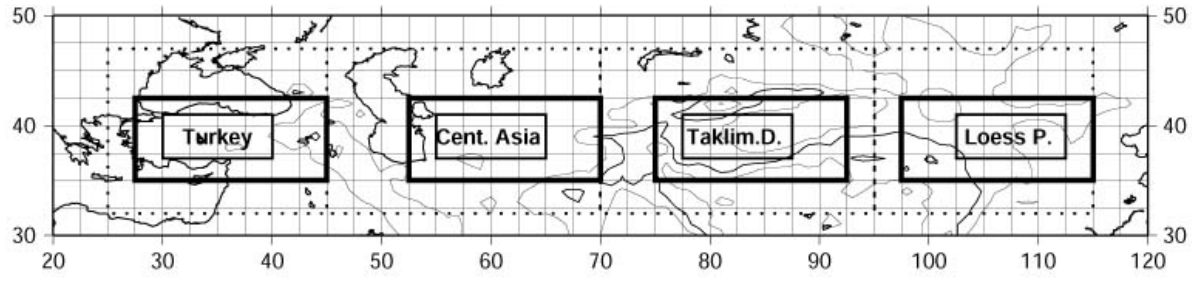

Fig.3 Geographical distribution of the box regions dicussed in Yatagai (2003).

3. Validation of precipitation datasets

Precise grid precipitation datasets as well as an objective (re)analysis dataset are needed to estimate the hydrological balance with the methods described in the previous section. Figure 4 shows July precipitation for the four sub-regions shown in Fig. 5. The precipitation test product (Xie, 2002) was interpolated from Global Telecommunication System (GTS) based precipitation data by Shepherd (1968) (shown in the black lines). This product is compared with CMAP and ERA15 precipitation. The precipitation test product and CMAP (green lines) data are similar except for the years 1979, 1980, and 1981 over the Tibetan Plateau. The ERA15 forecast corresponds well with the other two products over the Loess Plateau. However, it overestimates precipitation over the Tibetan Plateau, which causes an overestimate for the whole domain (Fig. 4a). The few gauge stations that there are on the Plateau are at relatively low altitudes; thus, the two products (test product and CMAP) may underestimate real precipitation amounts. More gauge precipitation data were incorporated for the second product (Xie et al., 2003, in this volume), so the estimates are expected to be better. Consideration of orographical effects on precipitation is an important focus for future study.

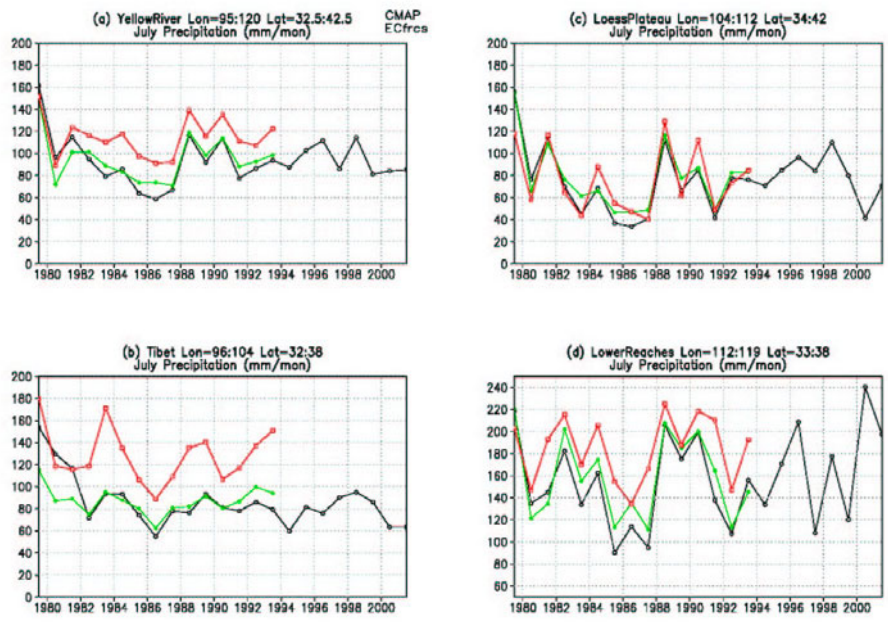

Fig. 4 July precipitation averaged for (a) the Yellow River domain, (b) Tibetan Plateau, (c) Loess Plateau and (d) Lower Reach of the Yellow River. The area is shown at the top of each panel and in Fig.5. Black: Xie (2002, test product), Green: CMAP (Xie and Arkin, 1997), Red: ERA15 forecasted precipitation.

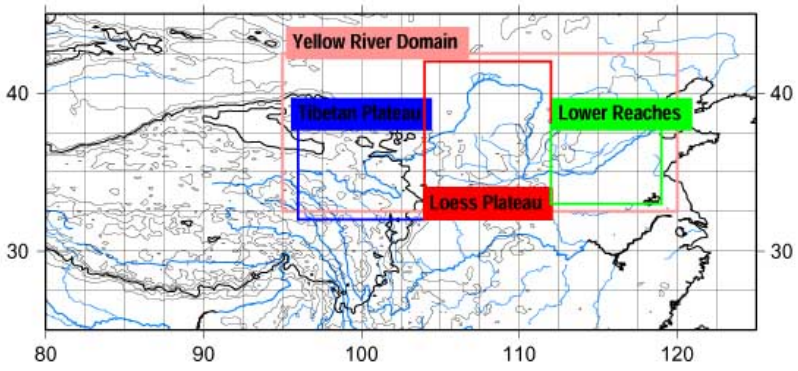

Fig.5 Geographical distribution of the Yellow River domain. (See Fig.4.)

4. Interannual variation of the hydrological budget

Figure 6 shows an example of interannual variability in July precipitation for the test product (black lines) and July moisture convergence derived from the ERA15 data. In general, the time series of convergence correspond to time series of precipitation.

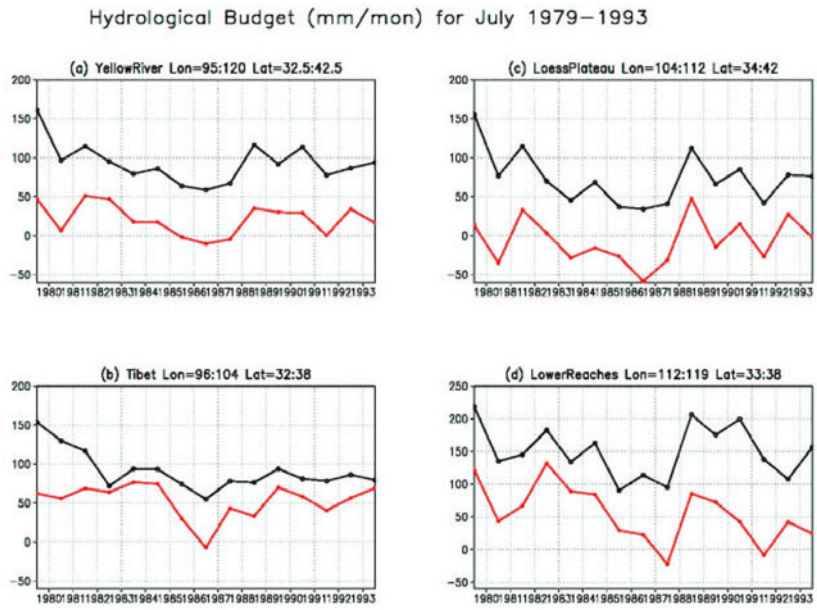

Fig.6 The interannual variations of precipitation (black lines) and atmospheric moisture convergence (red lines) averaged in the each dotted boxed shown in Fig. 5.

Negative convergence suggests that an area has more evaporation than precipitation at the surface. Thus, the difference between the two lines, namely (precipitation) – (convergence), represents the areal averaged evaporation, as shown in Fig. 2. Over the Tibetan Plateau, the areal averaged precipitation and convergence show similar values in 1982 and 1993. As the eastern part of the Tibetan plateau is a moisture source, these values may contain significant errors. Further investigation using better products is warranted.

In this note we showed the preliminary results of averaging precipitation or of convergence in the boxed areas shown in Figure 5. However, if we consider average parameters for a river basin (or sub-basin), convergence values can be compared to runoff if storage is neglected. Furthermore, if high quality datasets for moisture convergence, precipitation, and runoff are available, the average storage of water in a basin can be evaluated (e.g. Oki et al., 1995; Seneviratne et al. 2004; submitted).

References

Gibson JK, Kallberg P, Uppala S, Nomura A, Hernandez A, Serrano E. 1997. ERA Discription. *ECMWF re-analysis project report series*, **1**, 72pp.

Kalnay E, Kanamitsu M, Kistler R, Collins W, Deaven D, Gandin D, Iredell M, Saha S, White G, Woollen J, Zhu Y, Chelliah M, Ebisuzaki W, Higgins W, Janowiak J, Mo KC, Ropelewski C, Wang J, Leetmaa A, Rdynolds R, Jenne R, Joseph D. 1996. The NCEP/NCAR 40-year reanalysis project, *Bull. Amer. Meteor. Soc.*, **77**: 437-471.

Oki T, Musiake K, Matsuyama H, Masuda K, 1995. Global atmospheric water balance and runoff from large river basins. *Hydrological Processes*, **9**: 655-678.

Seneviratne, S.I., P. Viterbo, D. Luthi and C. Schar (2004) Inferring changes in terrestrial water storage using ERA-40 reanalysis data: The Mississippi River basin (in press).

Simmons, AJ and JK Gibson, 2000: The ERA-40 Project Plan. ERA-40 Project Report series, No.1, 62pp.

Xie P, Arkin PA. 1997. Global precipitation: A 17-year monthly analysis based on gauge observations, satellite estimates, and numerical model outputs. *Bull. Amer. Meteorol. Soc.*, **78**: 2539-2558.

Yatagai, A. (2003): Hydrological Balance and its Variability over the Arid/Semi-Arid Regions in the Eurasian Continent Seen from ECMWF 15-year Reanalysis Data, *Hydrological Processes*, **17**, 2871-2884.

Estimates of Downward Surface Radiation over China

Jianqing XU (FRSGC), Tadahiro HAYASAKA,
Kazuaki KAWAMOTO (RIHN), and Shigenori HAGINOYA (MRI)

1. Introduction

Jordan sunshine recorder is a kind of direct solar radiation recorder (**Fig.1**). Sunlight penetrates a small hole on the side of a copper cylinder, hitting light-sensitive paper inside. The paper is changed daily. The length of the burned line on the light-sensitive paper is a measure of the sunshine duration. This is a very simple observation method that needs no electricity and is easily maintained. However, the recorder may omit time when the sun is at low altitudes (about 5°in city and 2°in rural area). Solar radiation data have been recorded for more than 50 years over most areas of China. Downward surface solar and long-wave radiation fluxes can be derived from sunshine duration data using parameters from a Jordan sunshine recorder. In the past 20 years, satellite observations and routine surface meteorological observations have occurred simultaneously. Two principal factors drive the development of this method. Although satellite data can be used effectively to analyze the surface radiation budget, the time period covered by the satellite-based SRB dataset (NASA Langley Research Center) is insufficient for climatic analysis.

2. Calculation method

Routine meteorological datasets were used to estimate downward surface solar and long-wave radiation fluxes. Downward surface solar radiation flux was derived from sunshine duration data using parameters from a Jordan sunshine recorder. Downward surface long-wave radiation flux was estimated from the surface air humidity, temperature, and calculated downward surface solar radiation. The influence of topography or high altitude was also considered. Calculations were checked against in situ observations.

Fig. 2; Revising raw sunshine duration data. Solid lines are the seasonal changes of different solar altitudes (2°, 4°, …20°). Upper panel is Jiuquan (39°46'N, 98°29'E, 1477m asl), lower panel is Baingoin (31°22'N, 90°01'E, 4700m asl). Marks are Nobs/N0 on fine days. If a meteorological station is in a valley or surrounded by high buildings, the observed sunshine duration can be shorter than its true value. Observed raw data should be revised for such cases. At Jiuquan, the ratios of Nobs/N0 exceed 0.92 and the

marks can be put around 2°- 4°of the solar altitude: the meteorological observatory at Jiuquan is in a open area without nearby mountains or buildings, so N=NObs there.

Fig. 1. The Jordan sunshine recorder.

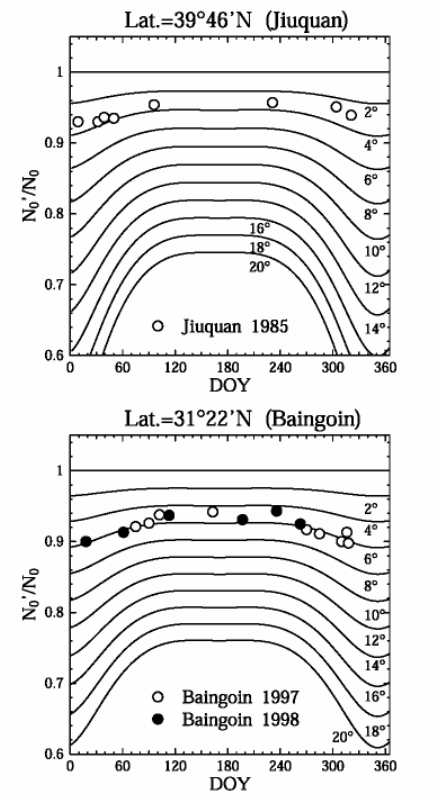

Fig. 2

Fig. 3; Seasonal changes in the ratios of sunshine duration Nobs/N0. Top panel is from the observed raw data, middle panel the revised data, and bottom panel the precipitation at Baingoin in 1998. At Baingoin, Nobs/N0 is sometimes less than 0.9, and the marks are placed between 4°- 7°. Sunlight is blocked when the solar altitude is less than about 5°. Baingoin may be in a valley on the Tibetan Plateau, and N≠NObs there.

Fig. 4; Seasonal changes in calculated solar radiation fluxes at Jiuquan in 1985. The solid line is the daily downward solar radiation SM↓, as estimated from sunshine duration. The dotted line is the daily downward solar radiation under clear sky conditions SMf↓ whenβDUST = 0.1. The broken line is SMf↓ when βDUST = 0.03. The dashed line is SMf↓ when βDUST = 0.0. WhenβDUST = 0.03, SMf↓adjusts SM↓ well. In winter, βDUST may be less than 0.03. In the present study, βDUST is assumed constant, with no seasonal changes.

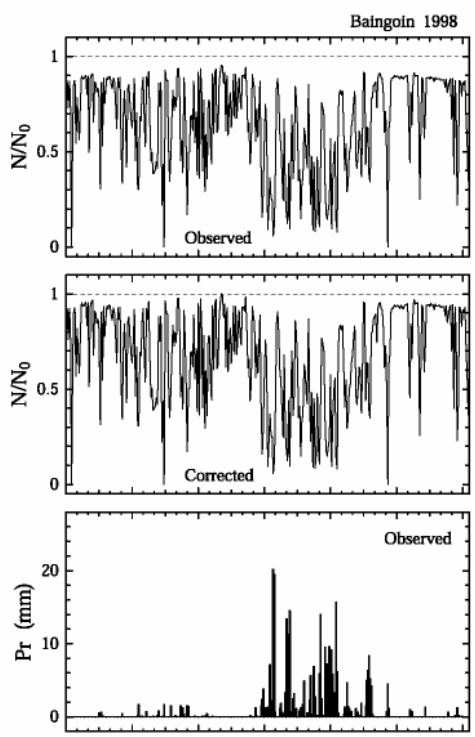

Fig.3

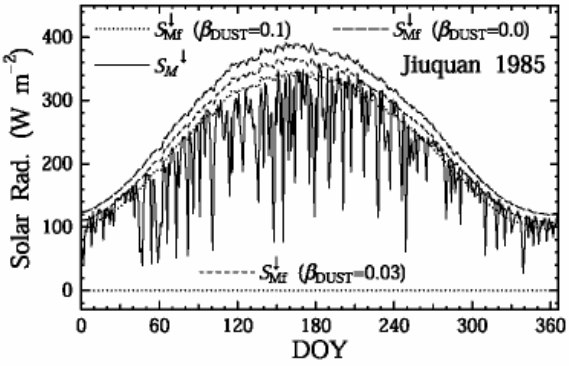

Fig.4

Fig. 5; The upper panel is the seasonal variation in solar radiation fluxes as observed by pyranometer and calculated from sunshine duration N for Lhasa in 1995. The solid line is the calculated SM↓ from N. The dotted line is SMf↓ under clear sky conditions with the Robinson's atmospheric turbidityβDUST = 0.02. Circles represent SM↓ observed by the pyranometer since 30 June 1995. The solar radiation ranges from about 100 Wm-2 to 380 Wm-2. Observed and calculated SM↓ agree. The lower panel shows the regression analysis of the observed and calculated SM↓. Regression analysis results suggest that the calculated values may be larger than observed values. Note, however, that data were observed only in the second half of the year.

Fig. 6; The left panel is the seasonal variation of the daily mean downward long-wave radiation flux LM↓ at Shiquanhe in 1998. Open circles are observed values and solid lines are calculated values. The right panel shows the regression analysis of the calculated and observed long-wave radiation. The calculations and observations agreevery well.

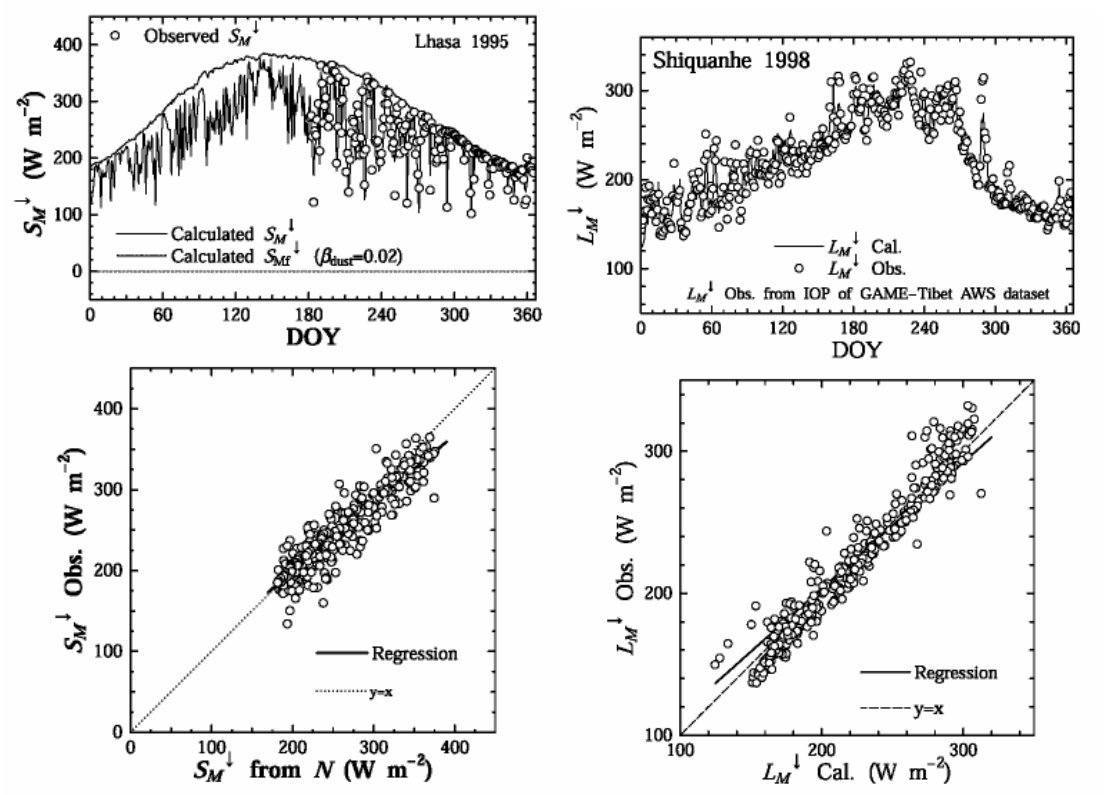

Fig. 5 **Fig.6**

3. Calculations and results

Calculations were performed for 31 stations in China. The calculation period was from 1971 to 2000. The Langley SRB dataset includes monthly means covering the period July 1983-June 1995 and was developed by the Radiation Sciences Branch of the Atmospheric Sciences Division at NASA, Langley Research Center, Hampton, Virginia. The irradiances are calculated using computationally fast radiative transfer algorithms whose primary input data are from the International Satellite Cloud Climatology Project (ISCCP) C1 products.

Fig. 7. Interannual variations in the surface radiation fluxes expressed by monthly mean values at Beijing from 1971-2000. The solid line is the monthly mean solar radiation SM↓, the dotted line is the long-wave radiation and the dashed line is the solar radiation from the Langley SRB dataset. The broken line and dotted chain are, respectively, SM↓and LM↓ trends obtained from line regression analysis. SM↓ changes from 83 Wm-2 (December) to 243 Wm-2 (February). The maximum and minimum monthly mean LM↓, 417 Wm-2 and 222 Wm-2, occur in July and January, respectively. Solar radiation has been decreasing at Beijing, perhaps as a result of increasing atmospheric

aerosols linked to its rapid development. Observed sunshine is also decreasing. Long-wave radiation has increased, and the rate of temperature change (Table 1) is large (0.0752 K yr-1).

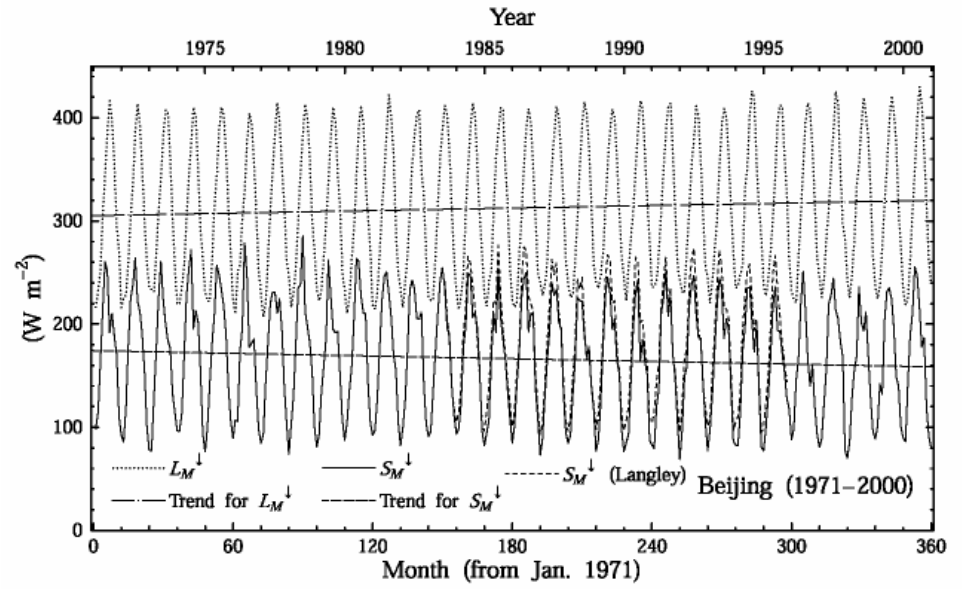

Fig. 7

Fig. 8. As in Fig.7, except for Hailar. Hailar (49.2°N, 119.8°E, 614m asl) is in rural northern China. SM↓and LM↓ are smaller than in Beijing. SM↓ changes from 47 Wm-2 (December) to 253 Wm-2 (June), LM↓ changes from 155 Wm-2 (January) to 360 Wm-2 (July). The mean values of SM↓ and LM↓ are 154 Wm-2 and 250 Wm-2, respectively (Table 1). SM↓ is decreasing and LM↓ is increasing.

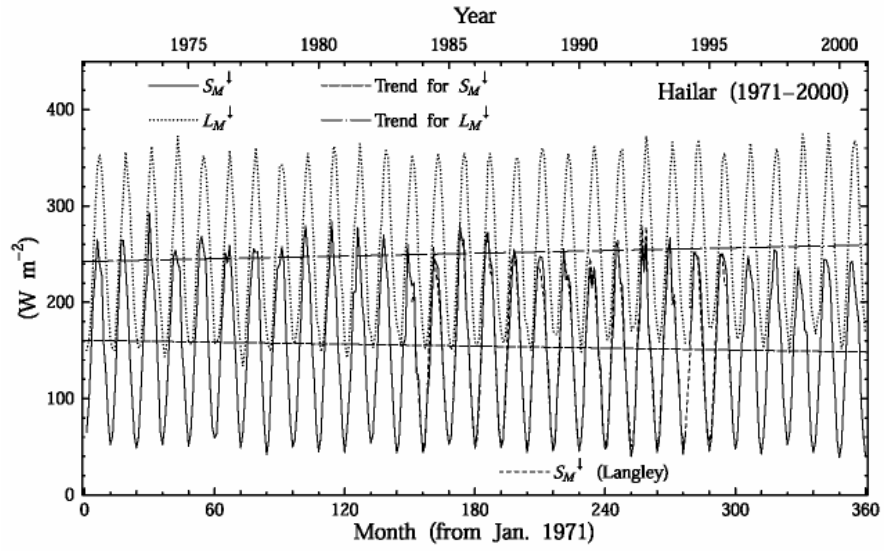

Fig.8

Fig. 9. As in Fig.7, except for Lhasa. Lhasa (29.7°N, 91.1°E, 3650m asl) is on the Tibetan Plateau. Variations in SM↓and LM↓ are very different from those at Beijing and Hailar. LM↓is larger than SM↓ at Beijing and Hailar, but they have similar values over Lhasa. As at Beijing and Hailar, SM↓is decreasing and LM↓ is increasing.

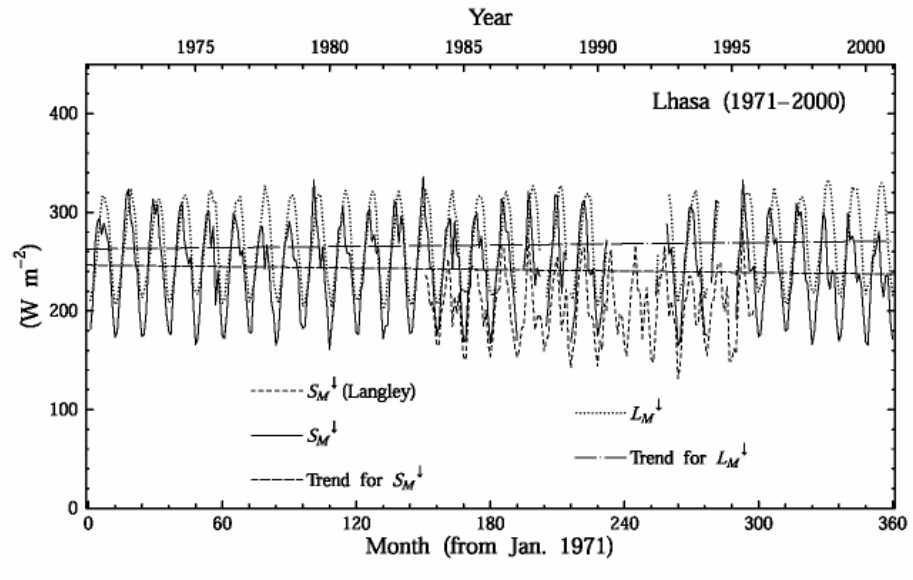

Fig.9

Fig. 10 The distribution of the solar radiation estimated from observed solar radiation duration for January, April, July, and October 1985.

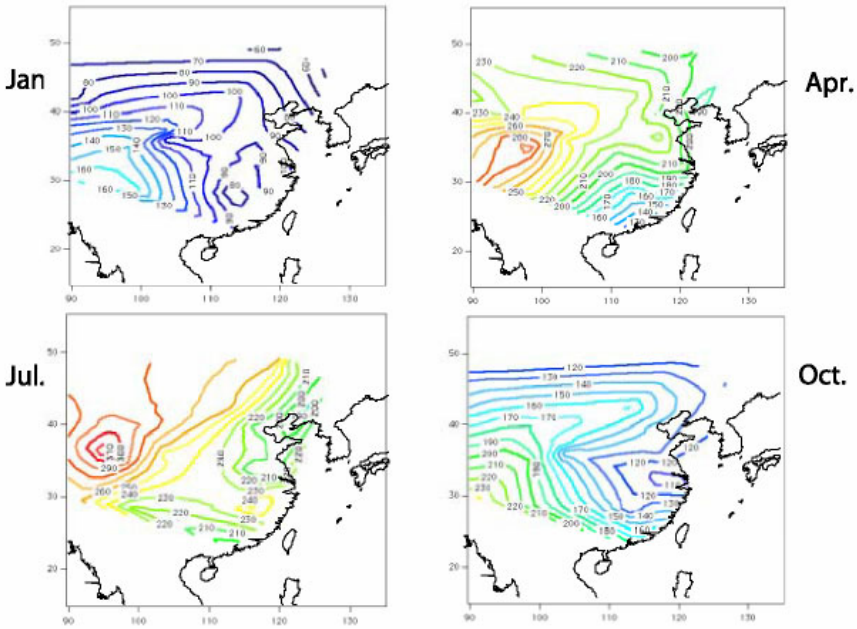

Fig.10

Table 1. Trends for each station from 1971-2000.

Name of the observatory	ΔT_A K yr^{-1}	Δe hPa yr^{-1}	ΔN hour yr^{-1}	$\Delta S_M^{\downarrow}$ Wm^{-2} yr^{-1}	$\Delta L_M^{\downarrow}$ Wm^{-2} yr^{-1}	$S_M^{\downarrow}$ Wm^{-2}	$L_M^{\downarrow}$ Wm^{-2}
Hailar	0.0777	0.02545	−11.692	−0.394	0.479	154.29	250.42
Bugt	0.0404	0.01313	6.893	0.216	0.076	154.75	248.37
Harbin	0.0648	0.02127	−12.971	−0.444	0.457	152.10	276.73
Altay	0.0461	0.02992	1.290	0.056	0.217	171.71	266.94
Fuyun	0.1024	0.00064	3.571	0.135	0.307	169.98	261.53
Urumqi	0.0220	−0.00152	−14.899	−0.474	0.259	168.47	282.33
Turpan	0.0641	−0.00941	−7.022	−0.220	0.323	172.01	315.24
Hotan	0.0359	0.01276	14.169	0.624	−0.030	184.78	302.76
Andir	0.0339	0.03613	−2.343	−0.113	0.261	190.51	289.11
Dunhuang	0.0372	0.00307	8.900	0.374	0.013	203.62	278.97
Jiuquan	0.0321	0.00606	5.639	0.248	0.067	198.18	272.48
Wushaoling	0.0387	0.00726	1.813	0.080	0.129	199.92	241.59
Golmud	0.0331	0.00253	3.633	0.165	0.072	223.00	251.98
Lanzhou	0.0659	−0.01633	−1.649	−0.047	0.250	183.00	294.91
Jurh	0.0524	−0.00135	−5.137	−0.208	0.273	194.86	260.38
Shenyang	0.0265	0.01047	−6.275	−0.273	0.202	155.02	297.60
Beijing	0.0752	−0.00576	−11.587	−0.484	0.436	166.42	312.52
Jinan	0.0358	0.02264	−16.855	−0.722	0.400	167.80	327.17
Lhasa	0.0384	0.00093	−7.313	−0.353	0.251	241.55	266.16
Madio	0.0372	0.00225	5.603	0.239	0.028	227.48	221.84
Deqen	0.0529	0.02371	−10.617	−0.480	0.406	196.93	274.31
Xi'an	0.0449	−0.01299	−25.995	−1.094	0.510	139.96	334.99
Lushi	0.0095	0.00414	6.512	0.276	−0.040	157.85	322.42
Changsha	0.0095	0.00342	−9.333	−0.437	0.188	136.47	355.89
Boxian	0.0332	0.00091	−14.941	−0.654	0.317	160.92	332.36
Dongtai	0.0334	0.00829	1.393	0.057	0.184	157.76	333.42
Hefei	0.0381	0.00213	−2.529	−0.110	0.213	148.49	342.90
Shanghai	0.0606	0.02051	−6.641	−0.300	0.417	148.33	344.56
Nanchang	0.0252	0.02585	−9.455	−0.436	0.278	149.85	354.02
Nanping	0.0285	0.01576	0.609	0.035	0.135	148.91	367.06
Guangzhou	0.0303	−0.00414	−14.647	−0.704	0.407	145.10	380.44

4. Summary and conclusion

(1) A method to estimate downward surface solar and long-wave radiation fluxes has been developed. The inputs are routine meteorological data. Fluxes were calculated at 31 stations in China using data from 1971 to 2000.

(2) Downward surface solar radiation flux was derived from sunshine duration data using parameters from a Jordan sunshine recorder. The surface long-wave radiation

flux was computed from the estimated solar radiation, the observed surface air humidity, and the temperature. Topographic influences and the effects of high altitude were considered. Calculations were verified by in situ observations.

(3) Over China, daily mean values of surface solar and long-wave radiation ranged from 140 - 240 Wm-2 and 220 - 380 Wm-2 , respectively. A map of the climatic distribution of surface solar radiation flux was presented.

(4) Climatic changes in the surface solar and long-wave radiation fluxes were investigated. The surface long-wave radiation flux at 29 out of 31 stations (Hotan and Lushi are the exceptions) has increased over the past 30 years. Surface solar radiation has decreased in large cities. Surface air temperature has increased at all 31 stations; vapor pressure has increased at most of the stations.

References

Kondo, J., and J. Xu, 1997: Seasonal variations in the heat and water balances for non-vegetated surfaces. J. Appl. Meteor., 36, 1676-1695.

Xu, J., and S. Haginoya, 2001: An estimation of heat and water balances in the Tibetan Plateau. J. Meteor. Soc. Japan, 71(1B),485-504.

Xu, J. 2001: An analysis of the climatic changes in the Eastern Asia using the potential evaporation, J. Japanese Soc. Hydro. And Water Resour., 14(2),151～170, (in Japanese with English summary)

Xu, J., S. Haginoya, K. Saito, and K. Motoya, 2003: Surface Heat and Water Balance Trends in Eastern Asia in the period 1971-2000. Hydrological Processes (in press)

Xu, J., S. Haginoya, K. Masuda, and R. Suzuki, 2004: An Estimation of heat and water balances over the Tibetan Plateau in 1997-1998. J. Meteor. Soc. Japan (in press)

Preliminary results on interactions between seawater, groundwater and river water in the Yellow River delta

Makoto Taniguchi[1], Shin-ichi Onodera[2], Kunihide Miyaoka[3], Tomochika Tokunaga[4], Jianyao Chen[1], and Guanqun Liu[5]

1: Research Institute for Humanity and Nature, Japan
2: Hiroshima University, Japan
3: Mie University, Japan
4: University of Tokyo, Japan
5: Ocean University of China, China

1. Introduction

The Yellow River does not reach often to the Bo-Hai Sea since 1990's because of huge amount of water uses for irrigation at midstream. Shortage of river water induces water pollution, decrease in groundwater level, and decrease of nutrient transports to the Bo-Hai Sea. Evaluations of riverwater–groundwater-seawater interactions are important for water and nutrient budgets (Taniguchi et al., 2002; Burnett et al., 2003). The purposes of this study are; (1) to evaluate groundwater and river water discharges and their dissolved material transports into the Bohai Sea, (2) to evaluate the effect of recent Yellow River cut-off due to changes in land utilization and water management on groundwater and Bohai Sea, and then (3) to evaluate the interactions between Yellow River, groundwater, and Bohai Sea in the delta.

2. Methods

Studies on land-ocean interaction in the Yellow River Delta are planed from 2003 to 2006 though; (a) measurements of chemical components of water in the Yellow River, and (b) investigations of the groundwater and coastal water in the Yellow River Delta. River water will be collected at Lijin for chemical analyses (DIN (NO3, NO2, NH4) , DIP, DON, DOP, TN, TP, Si, DO, pH, SPN) to evaluate the transports of dissolved materials to the Bo-Hai Sea through Yellow River. Interactions between groundwater and seawater in the Yellow River delta will be evaluated using 10 automated seepage meters,

CTD (Conductivity-Temperature-Depth) probes in 10 boreholes, resistivity cables, and fiber thermo-radars. Chemical analyses of submarine groundwater seepaged into Bo-Hai Sea will be made for isotope components (O-18, Deutrium, C-14, N-15), and dissolved components.

Feasibility studies in the Yellow River delta had been made on August 2002, and September 2003. Groundwater and water of the Yellow River in the delta were analyzed for isotope components and dissolved components (**Fig. 1**). Resistivities of the pore-water were also measured to evaluate seawater-groundwater and riverwater-groundwater interactions. Groundwater potential and electric conductivities were also measured using piezometer nests near the Yellow River and Bohai Sea to evaluate groundwater-river water and groundwater seawater interactions.

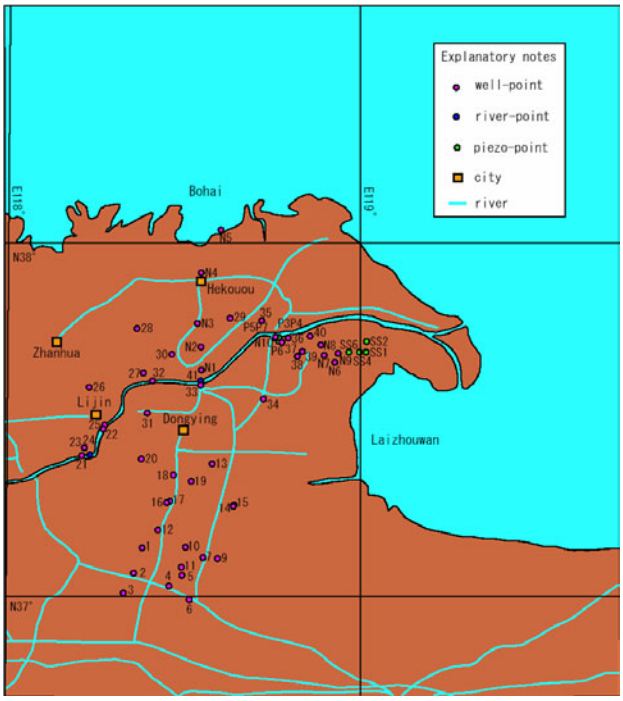

Fig. 1 Location of the study area and boreholes

3. Preliminary results

Electric conductivity of the groundwater in the south of the delta was 1.5 times larger than that of the current seawater. The stable isotope components show that the groundwater is the mixture of the meteoric water and seawater, but not current seawater (**Fig.2**)

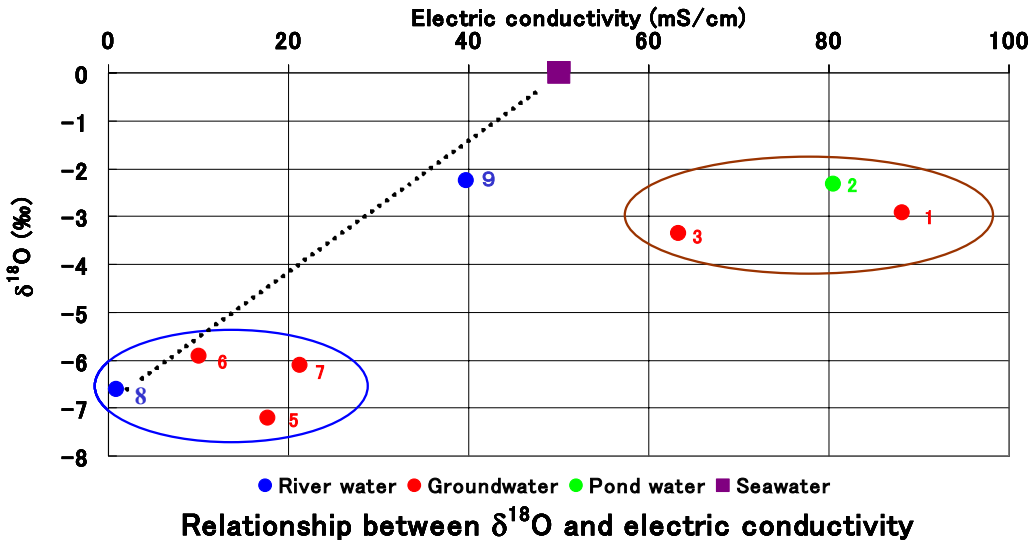

Fig. 2 Relationships between δ18O and conductivity of the waters in the Yellow River delta.

Fig. 3 shows the distribution of Na/Ca ratio along the line from the Yellow River (RS) to Bohai Sea (SS). The Na/Ca ratio increases with the distance from the Yellow River to the Bohai Sea.

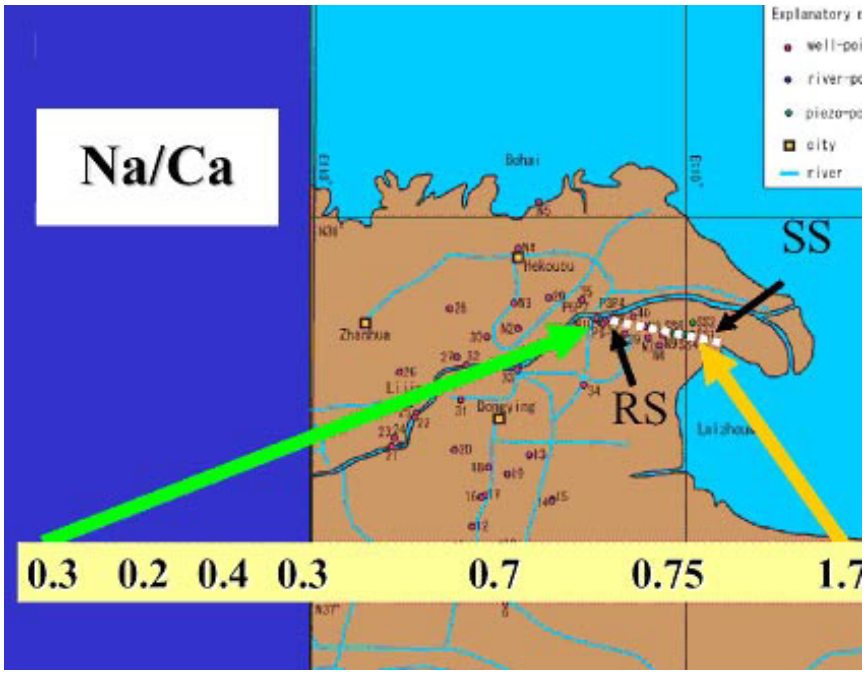

Fig. 3 Na/Ca distribution along the line from the Yellow River (RS) to Bohai Sea (SS)

In order to evaluate groundwater-river water and groundwater-seawater interactions, groundwater potential and electric conductivity were measured using piezometric nests near the Yellow River and near the Bohai Sea. **Fig 4** shows the hydraulic head and electric conductivity of the groundwater at (a) RS (**Fig 3**) and at (b) SS (**Fig.3**). The groundwater discharges from the Yellow River (**Fig. 4a**), and into Bohai Sea (**Fig.4b**). The electric conductivity increased along the groundwater flow line.

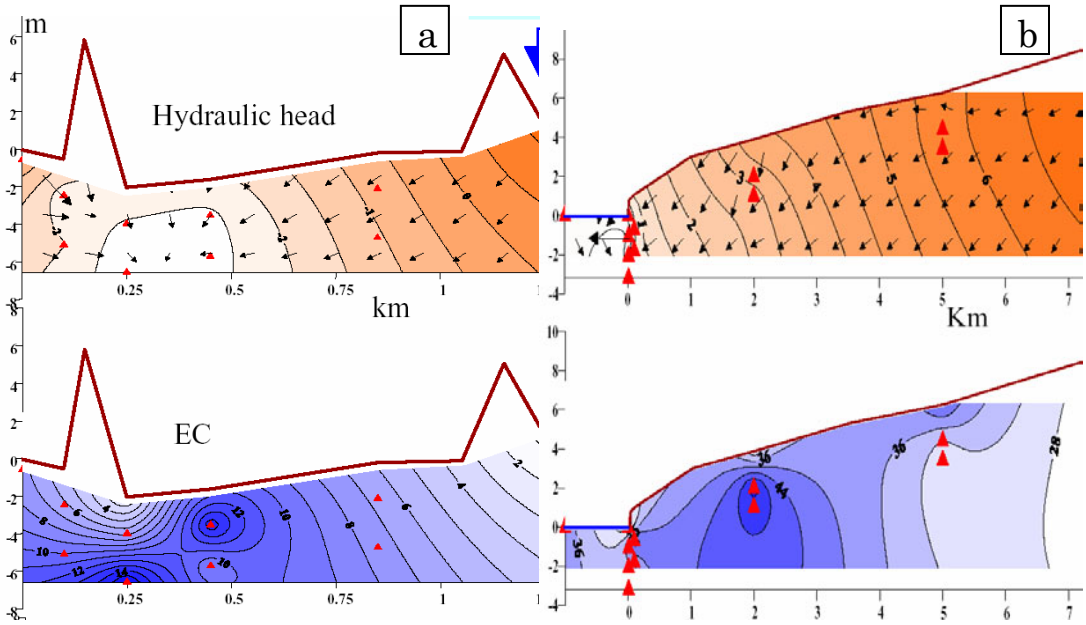

Fig.4 Hydraulic head and electric conductivity (a) near the Yellow River (RS) and (b) near the Bohai Sea (SS). The Yellow River is located at the right of **Fig 4a**, and Bohai- sea is located at left of **Fig. 4b**.

The pore-water resistivities were measured using resistivity cable to evaluate seawater-freshwater interface. **Fig 5** shows that the fresh water exists in the shallow aquifer and salty water is located in the deep aquifer. The resistivity of the pore-water in the inland is higher (conductivity is lower) than that near the coast at the same depth.

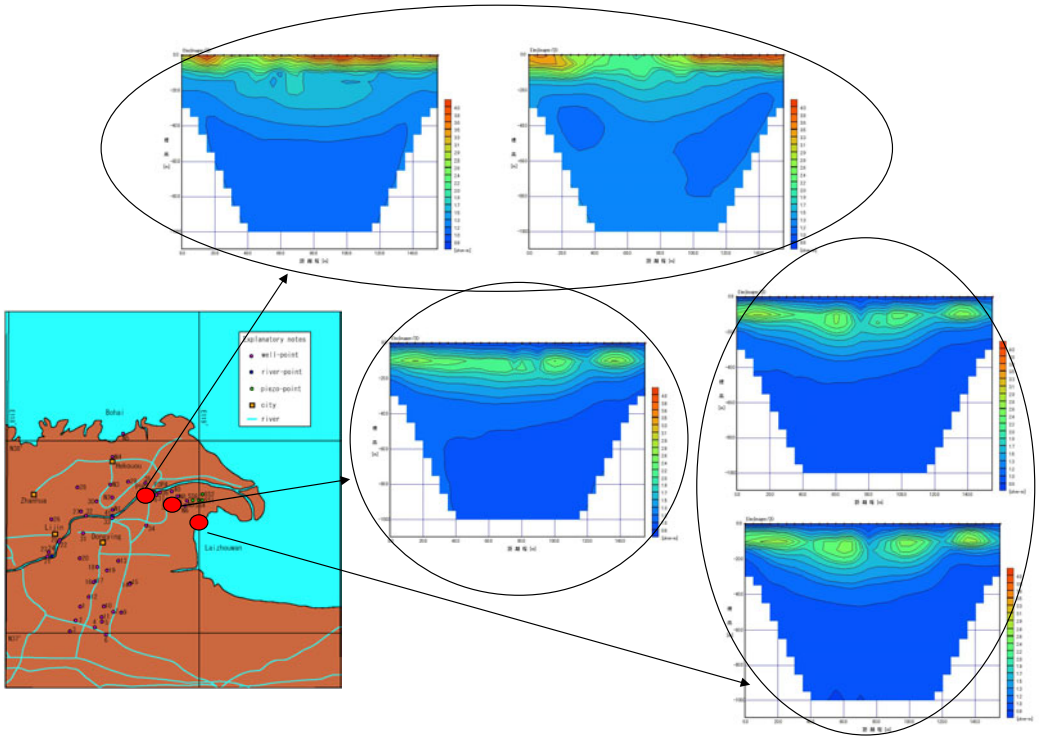

Fig. 5 Pore-water resistivity in the Yellow River delta.

References

Burnett, W.C., H. Bokuniewicz, M. Huettle, W.S. Moore, and M. Taniguchi. 2003. Groundwater and pore water inputs to the coastal zone. Biogeochemistry. 66, 3-33.

Taniguchi, M., W.C. Burnett, J.E. Cable, J.V. Turner. 2002. Investigation of submarine groundwater discharge. Hydrol. Process. 16, 2115-2129.

V List of related meetings

(1) AOGS (Asia Oceania Geosciences Society) Meeting

5-9, July 2004, Suntec Singapore, Singapore

Land-Ocean Interactions in Asia and Oceania (IWG4)

Conveners: Makoto Taniguchi (RIHN), Ming H Wong (Hong Kong Baptist University), and Lawrence Koe (Nanyang Technological University)

http://www.asiaoceania.org/index.html

(2) WPGM (Western pacific Geophysics Meeting)

16-20 August 2004 (Monday-Friday), Honolulu, Hawaii

Integrations of hydrological studies on atmosphere-land-ocean interactions (H04)

Conveners: Tetsuya Hiyama (HyARC), and PingPing Xie (NOAA)

http://www.agu.org/meetings/wp04/

(3) International Workshop of the Yellow River Studies

November, 2004, Shiga, Japan

Organizers: Yoshihiro Fukushima (RIHN) and Changming Liu (CAS)

Yoshihiro Fukushima, Project Leader
Makoto Taniguchi, Secretary General
Research Institute of Humanity and Nature (RIHN), Inter-University Research Institute
Ministry of Education, Culture, Sports, Sciences, and Technology, Japan (MEXT)

335 Takashima-cho, Kamigyo-ku, Kyoto 602-0878, Japan
Tel: +81-75-229-, Fax: +81-75-229-6150
E-mail: YRiS@chikyu.ac.jp, URL: http://www.chikyu.ac.jp/index_e.html